Environmental Science and Pollution Research (2019) 26:5094–5110
https://doi.org/10.1007/s11356-018-3989-4

RESEARCH ARTICLE

Adsorption performance and mechanisms of Pb(II), Cd(II), and Mn(II) removal by a β-cyclodextrin derivative

Mengjiao Zhang[1] · Liyun Zhu[2] · Changhua He[1] · Xiaojun Xu[1] · Zhengyang Duan[1] · Shuli Liu[1] · Mingyao Song[1] · Shumin Song[1] · Jiemei Shi[1] · Yu'e Li[1] · Guangzhu Cao[3]

Received: 10 August 2018 / Accepted: 12 December 2018 / Published online: 3 January 2019

Abstract

In this study, the novel adsorbent PVA-TA-βCD was synthesized via thermal cross-linking between polyvinyl alcohol and β-cyclodextrin. The characterization methods SEM-EDS, FTIR, and XPS were adopted to characterize the adsorbent. The effect of pH, contact time, initial concentrations, and temperature during the adsorption of Pb(II), Cd(II), and Mn(II) onto the PVA-TA-βCD was also investigated. In a single-component system, the data fitted well to pseudo-second-order, and film diffusion and intra-particle diffusion both played important roles in the adsorption process. As for isotherm study, it showed a heterogeneous adsorption capacity of 199.11, 116.52, and 90.28 mg g^{-1} for the Pb(II), Cd(II), and Mn(II), respectively. Competition between the ions existed in a multi-component system; however, owing to the stronger affinity of the PVA-TA-βCD for Pb(II) relative to Cd(II) and Mn(II), the Pb(II) adsorption onto the PVA-TA-βCD was less affected by the addition of the other metals, which could be effectively explained by the hard and soft acid and base theory (HSAB). Furthermore, PVA-TA-βCD showed good reusability throughout regeneration experiments.

Keywords Heavy metal · Chelation · Electrostatic attraction · Adsorbent · Multi-component · Wastewater treatment

Introduction

Currently, large amounts of wastewater containing toxic inorganic substances, such as heavy metals, are released into the environment daily, and this has drawn increasing attention due to continuing industrialization (Jia et al. 2016; Borsagli et al. 2015). Heavy metal ions accumulate easily in living organisms and pose a serious threat to human health. Lead directly injures human brain cells, and cadmium adversely affects the brain, reproductive organs, skeletal system, and kidneys (Luo et al. 2014; Xu et al. 2015). Manganese is essential for normal bone formation, but excessive intake can easily cause neurotoxicity, resulting in dystonia, bradykinesia, rigidity, tremors, and other symptoms (Chen et al. 2016b). As such, it is important to explore novel methods for reducing the concentration of toxic metal ions in industrial effluents, allowing such industries to reach set discharge standards. Compared with other methods that have been used to remove heavy metal ions from effluents, such as filtration, chemical precipitation, ion exchange, and electrochemical treatments (Liu et al. 2018; Heidari et al. 2009), adsorption presents as a more desirable method due to its high efficiency, low cost, simplicity of operation, and the absence of sludge byproducts or secondary contaminants (Grujić et al. 2017; Kyzas et al. 2015). However, many traditional adsorbents, such as commercial activated carbon, zeolites, and clay biomass, present some disadvantages (Crini 2005). For example, adsorbents with a high adsorption capacity also have a relatively high cost, and low-cost adsorbents typically have a weak ability to bind heavy metal ions (Liang et al. 2017).

Responsible editor: Tito Roberto Cadaval Jr

✉ Liyun Zhu
lyunzhu@126.com

[1] Faculty of Environmental Science and Engineering, Kunming University of Science and Technology, Kunming 650500, People's Republic of China

[2] Faculty of Foreign Languages and Cultures, Kunming University of Science and Technology, Kunming 650500, People's Republic of China

[3] Faculty of Land Resource Engineering, Kunming University of Science and Technology, Kunming 650500, People's Republic of China

β-cyclodextrin (β-CD) has the characteristics of low cost, biocompatibility, and high hydroxyl group content; therefore, this compound has attracted substantial interest for use as an adsorbent (He et al. 2018). However, natural β-CD is difficult to separate from aqueous solutions; as such, β-CD must be modified in order to function successfully as an adsorbent of heavy metal ions. Modified β-CD can acquire reduced solubility and increased stability in two ways: the β-CD can be attached as a pendant group on polymer chains, and the β-CD can be associated with bifunctional cross-linkers (Girek and Ciesielski 2011). It has been reported that modified β-CDs, such as EDTA-cross-linked β-CD (Zhao et al. 2015a), Fe_3O_4/cyclodextrin polymer nanocomposites (Badruddoza et al. 2013), and sericin/β-CD/PVA composite electrospun nanofibers (Zhao et al. 2015b), can be used for adsorbing a variety of dyes and heavy metal ions from industrial wastewater. In this study, a thermal cross-linking method was used to cross-link the hydroxyl group of β-CD with the carboxyl group of a cross-linking agent, and polyvinyl alcohol (PVA) was used to immobilize the β-CD due to its good mechanical strength (Jing and Li 2016). Based on the hard and soft acid and base (HSAB) theory, Pb(II) is classified as a soft acid, whereas Cd(II) and Mn(II) are classified as intermediate acids. Therefore, these three ions could combine with soft ligand groups, such as –SH (Wang and Chen 2009). To this end, we attempt to use thiomalic acid (TA) containing –SH and –COOH as a cross-linking agent.

This manuscript focuses on preparing a high mechanical strength and good selectivity β-CD derivative for use as an adsorbent for removing Pb(II), Cd(II), and Mn(II) from wastewater (Fig. 1). The adsorption behavior of PVA-TA-βCD including kinetics, isotherm, competitive adsorption, and the recyclability of the adsorbent was studied. The mechanism of heavy metals onto PVA-TA-βCD was investigated via scanning electron microscopy/energy-dispersive spectroscopy (SEM-EDS), zeta potential, Fourier-transform infrared spectra (FTIR), and X-ray photoelectron spectroscopy (XPS).

The experimental section

Materials

β-CD ($C_{42}H_{70}O_{35}$; illustrated in Fig. 1), PVA ($[C_2H_4O]_n$), and TA ($C_4H_6O_4S$; illustrated in Fig. 1) were provided by Aladdin Biochemical Technology. Sodium dihydrogen phosphate (NaH_2PO_4), manganese chloride ($MnCl_2$), cadmium chloride ($CdCl_2$), and lead chloride ($PbCl_2$) were purchased from Tianjin Fengchuan Chemical Reagent Technologies Co., Ltd. Na_2EDTA was obtained from Sinopharm Chemical Reagent Co., Ltd. All reagents were of analytical reagent grade and were used directly in the experiment without further purification.

Preparation of PVA-TA-βCD

The preparation of the PVA-TA-βCD required three processes: first, β-CD (1 g) and PVA as the skeleton (0.1 g) were added to 25 mL of ultrapure water, and the mixture was then placed in a water bath cauldron at 363 K and stirred until the material had completely dissolved. After this, the cross-linking agent TA (0.6 g) and the catalyst NaH_2PO_4 (0.05 g) were added to the mixture, and the reaction was continued for 1 h in a water bath cauldron at 363 K. Subsequently, the reaction solution was transferred from the water bath pot to an oven for thermal cross-linking at 413 K for 4 h to ensure thermal cross-linking was completed. The light yellow solid reactants were ground into a powder in a mortar, sieved through a 100-mesh sieve, and repeatedly washed with ultrapure water. Finally, the synthetic products were placed into an oven to dry at 353 K overnight prior to further use.

Adsorption of heavy metal ions

The stock metal solutions (1000 mg L^{-1}) were prepared by dissolving the appropriate masses of metal salts in ultrapure

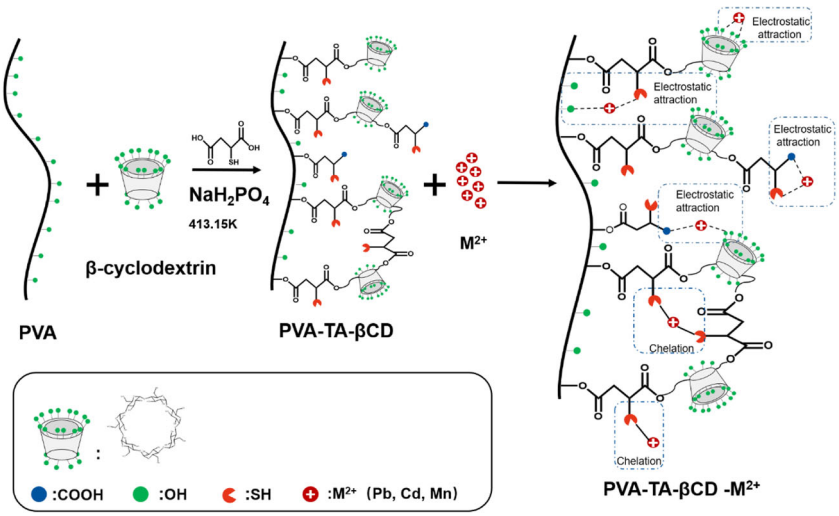

Fig. 1 The preparation of the PVA-TA-βCD and the adsorption mechanism towards Pb(II), Cd(II), and Mn(II) ions

water, and the other concentrations of heavy metal ions were diluted from this stock solution. The batch adsorption experiments were conducted using 0.02 g of adsorbent in a 30 mL solution of Pb(II), Cd(II), and Mn(II) and were stirred in a thermostatic shaker at 120 rpm for 180 min. To determine the effect of pH on adsorption, the pH was adjusted from 2 to 6 using 0.1 mol L^{-1} NaOH and 0.1 mol L^{-1} HCl at an initial concentration of 100 mg L^{-1}. The kinetic experiments were performed by varying the contact time from 5 to 180 min with an initial concentration of 100 mg L^{-1}. The sorption isotherms of M^{2+} (M: Pb, Cd, Mn) for the PVA-TA-βCD were determined using a batch equilibration technique with M^{2+} concentrations ranging from 25 to 300 mg L^{-1}. The sorption thermodynamic experiments were conducted at an initial concentration of 100 mg L^{-1} and temperatures ranging from 298 to 328 K. In the multi-component adsorption experiments, either 2 or 3 types of the investigated M^{2+} were added at the same concentration (each 100 mg L^{-1}) to a 30 mL solution contained in a vial.

Before the test, the sorbents were filtered from the solution using 0.45-μm nylon sterile filters, and the filtrate was diluted by mixing it with ultrapure water. Subsequently, the concentrations of the above mixture solutions were measured using a flame atomic absorption spectrometer (AAS).

All experimental results were conducted in triplicate and averaged to reduce the experimental error and increase the accuracy. The equilibrium adsorption capacity (q_e, mg g^{-1}) (Eq. (1)) was calculated as follows:

$$q_e = \frac{(C_0 - C_e)V}{m} \tag{1}$$

where C_0 and C_e (mg L^{-1}) are the initial and the equilibrium concentrations of the heavy metal ions in aqueous solution, respectively, V (L) is the volume of the solution, and m (g) is the mass of the PVA-TA-βCD.

Statistical analysis

Besides the correlation coefficient (R^2), the residual root-mean-square error (RMSE) and the nonlinear chi-square test (χ^2) were used to evaluate the fitness of the kinetic and isotherm models relative to the experimental data (Baghdadi et al. 2016).

RMSE:

$$\mathrm{RMSE} = \sqrt{\frac{1}{N-2}\sum_{i=1}^{N}\left(q_{e,exp} - q_{e,cal}\right)^2} \tag{2}$$

The chi-square test (χ^2):

$$\chi^2 = \sum_{i=1}^{N}\frac{\left(q_{e,exp} - q_{e,cal}\right)^2}{q_{e,cal}} \tag{3}$$

where $q_{e,exp}$ and $q_{e,cal}$ (mg g^{-1}) are the experimental and the calculated values according to the model, respectively, and N is the number of experimental data. The smaller the RMSE value, the better the curve fitting. If data from the model are similar to the experimental data, χ^2 will be a small number.

Characterization of the materials

SEM-EDS (S4800, Hitachi) was used to observe the changes in the surface morphology and analyze the chemical elemental composition of the PVA-TA-βCD before and after adsorption. The chemical bonds and functional groups of the samples were determined via FTIR (NICOLET 5700, Thermo) in the range of 4000–400 cm^{-1} with KBr as a dispersant. XPS (ESCALAB 250XI, Thermo) was conducted to determine the elements. The zeta potentials of the PVA-TA-βCD at different pH values were measured using a zeta potential analyzer (ZEN3500, Malvern).

Desorption and regeneration

The desorption experiments were conducted using three eluents (0.01 M HCl, 0.01 M HNO_3, and 0.1 M Na_2EDTA), then the desorption kinetics and regeneration experiments were performed using the optimal eluents to study the desorption process and reproducibility of the saturated PVA-TA-βCD loaded with heavy metals. The desorption kinetics were conducted at various times. For the regeneration experiments, the PVA-TA-βCD was collected by centrifugation after desorbing, repeatedly washed with ultrapure water, and dried at 353 K for the next adsorption cycle. Reusability was assessed following the above adsorption-desorption process for four cycles in the presence of heavy metal ions. After every cycle, the adsorption capacity and desorption efficiency were calculated.

The desorption efficiency (%) (Eq. (4)) was calculated as follows:

$$\text{Desorption efficiency}\ (\%) = \frac{C'_e \cdot V}{m \cdot qe} \times 100\% \tag{4}$$

where C'_e (mg L^{-1}) is the equilibrium concentrations of the heavy metal ions in the aqueous solution after desorption, V (L) is the volume of the solution, m (g) is the mass of the saturated PVA-TA-βCD loaded with heavy metals, and q_e (mg g^{-1}) is the equilibrium adsorption capacity.

Results and discussion

Characterization of PVA-TA-βCD

SEM is a characterization technique that is frequently used to measure the surface morphology and other properties of

adsorbents (Ali et al. 2016), and EDS is commonly used to analyze an adsorbent's surface elemental content. Figure 2a shows the surface morphology of the adsorbent. The surface of the PVA-TA-βCD was mostly irregular and full of holes, owing to the bubbles produced during the thermal cross-linking. In contrast, the surface became smooth, and the number of pores decreased after the heavy metal ions were adsorbed (Fig. 2b), and this may be attributed to the likelihood that the Pb(II), Cd(II), and Mn(II) ions form complexes with the –SH of the adsorbent, then the complexes as nucleation sites promoted deposition of heavy metals, lastly the hydrolysis product of above complexed precipitated on the surface of PVA-TA-βCD (Wang et al. 2017). The EDS results are shown in Fig. 2c and indicate that the adsorbent contained C, O, S, and P. Among these, the S originated from the –SH in the TA and the P originated from the catalyst NaH_2PO_4. As such, we initially concluded that the TA successfully crossed-linked with the PVA and β-CD to form the insoluble PVA-TA-βCD. A comparison of the EDS results before and after adsorption (Fig. 2d) provided further direct evidence that the Pb(II), Cd(II), and Mn(II) had been adsorbed onto the surface of the PVA-TA-βCD.

Batch experiments

Effects of pH

It is well known that the adsorption process and the adsorption capacities of the adsorbents are different at different pH values due to the changes in the nature of the charged properties on the adsorbent's surface and the ion form in the solution (Zhao et al. 2015b; Pang et al. 2011). The zeta potential describes the nature of the charge of a material. As shown in Fig. 3a, the zeta potential of the PVA-TA-βCD was positive when the pH value was below the point of zero charge ($pH_{zpc} = 2.53$). The results showed that when the pH was > 2.53, the PVA-TA-βCD had a negative charge, which improved its ability to adsorb the heavy metals with a positive charge (Oladipo et al. 2015). Additionally, the pKa values of the carboxylic groups (3.8–5.0) (Vaghetti et al. 2009; Hu et al. 2017), thiol groups (3.5–9.3) (Yu et al. 2014), and hydroxyl groups (8–12) (Xu et al. 2011), when the pH was lower than pKa, would preclude the dissociation of the functional groups, and further adsorption of the heavy metal ions would be ceased. However, when the pH value is very high in an alkaline environment, heavy metal ions easily form metal hydroxides, and this

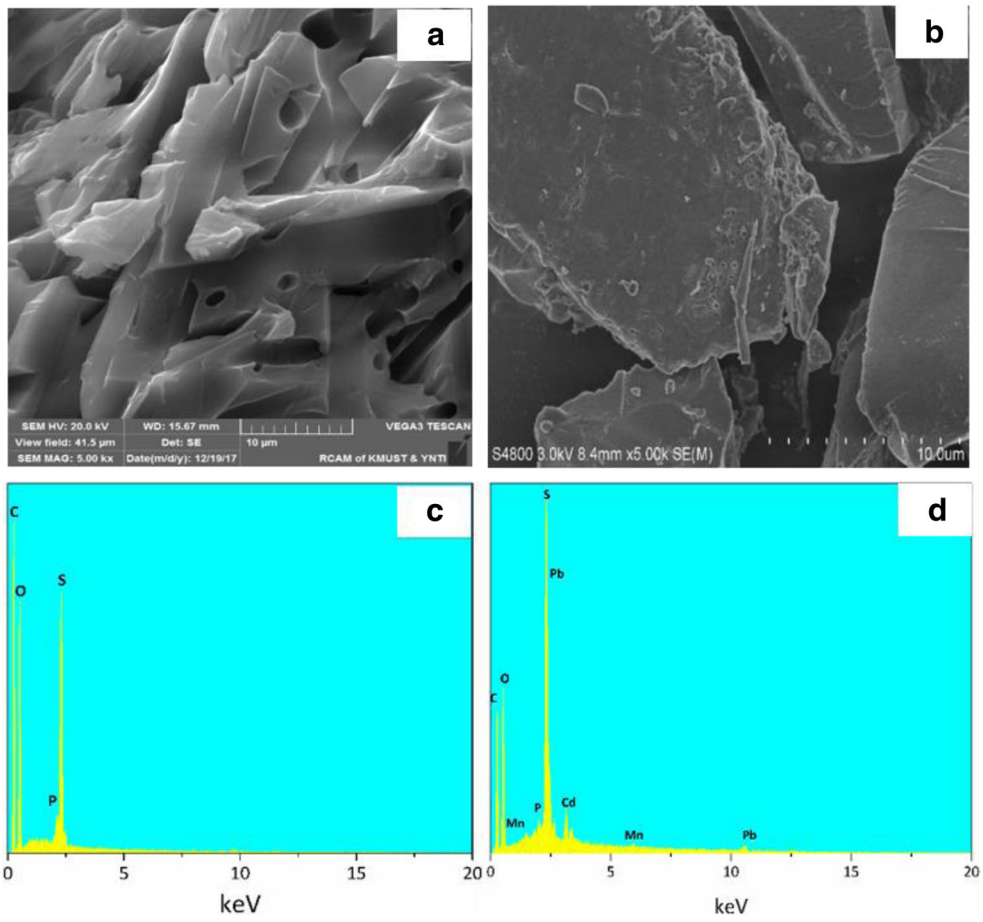

Fig. 2 SEM images and EDS spectra of the samples. **a** and **c** PVA-TA-βCD. **b** and **d** PVA-TA-βCD after Pb(II), Cd(II), and Mn(II) adsorption

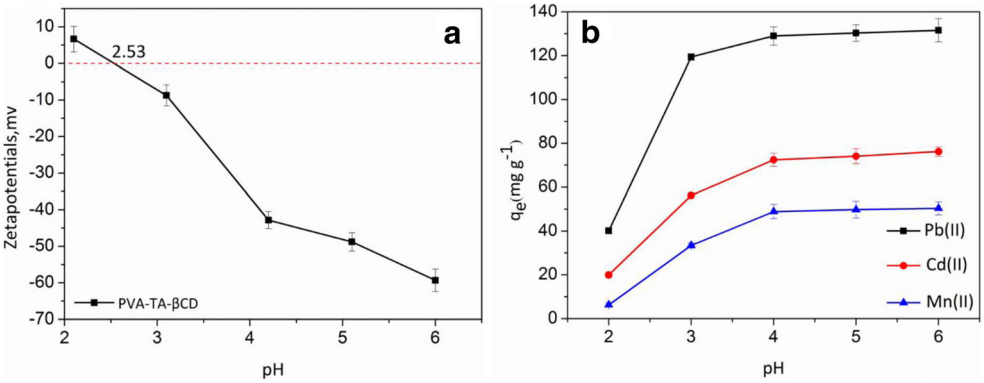

Fig. 3 **a** Zeta potentials of PVA-TA-βCD at different pH values. **b** Effect of pH on the uptake of Pb(II), Cd(II), and Mn(II) (conditions: initial metal concentration, 100 mg L^{-1}; solution volume, 30 mL; adsorbent dosage, 0.02 g; solution pH, 2–6; contact time, 180 min; temperature, 298 K; and shaking speed, 120 rpm)

phenomenon can result in inaccurate results in terms of evaluating the properties of the adsorbent.

Based on the above information, we investigated the adsorption performance of the PVA-TA-βCD for Pb(II), Cd(II), and Mn(II) at pH 2–6, a temperature of 298 K, and an initial ion concentration of 100 mg L^{-1}. Figure 3b indicates that the uptake capacities increased as an initial pH increased from 2 to 6. This occurred because the novel materials were protonated at pH 2 (Liang et al. 2009), generating a repulsive force between the adsorption site with a positive charge and the heavy metal ions with the same charge (Feizi and Jalali 2015). In addition, H^+ competes with the heavy metal ions in the aqueous solution to react with the adsorption sites of the adsorbent; therefore, the adsorption activity was low under these conditions. At pH 3–6, the metal uptake capacity increased sharply due to the enhanced deprotonation effect and that the PVA-TA-βCD surface was negatively charged, which generated a strong affinity for the heavy metal ions. As such, the functional groups would easily combine with the metal ions through electrostatic forces and chelation. The adsorption capacities were 130.31, 74.10, and 49.80 mg g^{-1} for Pb(II), Cd(II), and Mn(II) at pH = 5, respectively, and 131.55, 76.20, and 50.40 mg g^{-1} for Pb(II), Cd(II), and Mn(II) at pH = 6, respectively. There was no obvious change in the uptake capacities at a pH between 5 and 6, and the pH of ultrapure water was about 5.5, so the follow-up experiments did not require further adjustment to pH.

Adsorption kinetics

The adsorption kinetic results are based on the relationship between the metal ion uptake capacity of the materials and the contact time. Figure 4 shows that the adsorption capacities of the PVA-TA-βCD for the Pb(II), Cd(II), and Mn(II) ions in solution increased with increasing contact time, and the adsorption equilibrium was reached in all cases within 60 min. For further study of the adsorption process over time, a pseudo-first-order kinetic model (Eq. (5)) and a pseudo-second-order kinetic model (Eq. (6)) were used to fit the experimental data.

$$q_t = q_e\left(1-e^{-k_1 t}\right) \tag{5}$$

$$\frac{t}{q_t} = \frac{1}{k_2 q_e^2} + \frac{1}{q_e}t \tag{6}$$

where k_1 (min^{-1}) and k_2 (g mg^{-1} min) are the rate constants for the pseudo-first order reaction and the pseudo-second-order reaction, respectively, and q_e (mg g^{-1}) and q_t (mg g^{-1}) are the amounts of the adsorbed heavy metals at equilibrium and at time t, respectively.

The plots and corresponding kinetic parameters of these two models are shown in Fig. 4 and Table 1. It was observed that the pseudo-second-order model exhibited a better fit than the pseudo-first-order model. In addition, the calculated adsorption capacity values from the pseudo-second-order model were more consistent with the experimental values than the pseudo-first-order model. These results implied that a chemical reaction occurred between the heavy metals in solution and the adsorbents (Wang et al. 2015; Chen et al. 2016a).

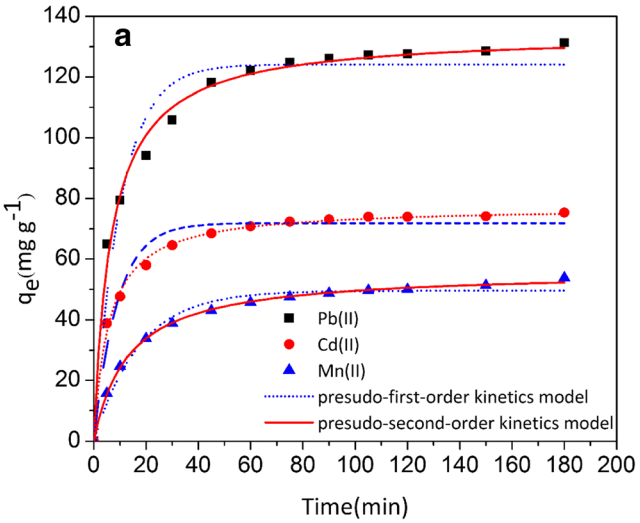

Fig. 4 Pseudo-first-order and pseudo-second-order sorption kinetics for Pb(II), Cd(II), and Mn(II) adsorption on the PVA-TA-βCD (conditions: initial metal concentration, 100 mg L^{-1}; solution volume, 30 mL; adsorbent dosage, 0.02 g; solution pH, 5.5; contact time, 5–180 min; temperature, 298 K; and shaking speed, 120 rpm)

Table 1 Adsorption kinetic parameters of Pb(II), Cd(II), and Mn(II) on PVA-TA-βCD

Metals	C_0 (mg L^{-1})	q_{exp} (mg g^{-1})	Pseudo-first-order					Pseudo-second-order				
			q_{cal} (mg g^{-1})	k_1 (min^{-1})	R^2	RMSE	χ^2	q_{cal} (mg g^{-1})	k_2 (g mg^{-1} min^{-1})	R^2	RMSE	χ^2
Pb(II)	100	131.25	124.11	0.099	0.955	7.969	9.378	134.39	0.00112	0.992	3.371	1.597
Cd(II)	100	75.30	71.83	0.113	0.968	3.858	1.189	77.27	0.00227	0.997	3.468	0.347
Mn(II)	100	53.88	49.63	0.058	0.979	2.350	2.022	56.14	0.00135	0.999	0.552	0.074

The intra-particle diffusion model and Boyd model were used to determine the diffusion mechanisms.

The intra-particle diffusion model is presented as follows:

$$q_t = k_i t^{\frac{1}{2}} + C \tag{7}$$

where q_t (mg g^{-1}) is the adsorption amount at time t (min), k_i (mg g^{-1} $min^{-1/2}$) is the intra-particle diffusion rate constant, and C is the intercept.

The adsorption process usually consists of three steps: diffusion of the sorbate through the boundary layer to the surface of the sorbent, intra-particle diffusion, and binding to the surface functional groups (Moulahcene et al. 2015). The adsorption equilibrium stage is commonly reached quickly and considered negligible, so the rate-controlling step of adsorption always involves film diffusion or intra-particle diffusion (Ozdes et al. 2011). As shown in Fig. 5a, it can be seen that all the heavy metal ions exhibited three distinct steps. The first step represents the film diffusion, which is the diffusion of the heavy metal ions through the boundary layer to the surface of the PVA-TA-βCD. The second part represents the intra-particle diffusion, and the third part is regarded as adsorption of the heavy metal ions to the functional groups on the internal surface of the adsorbent. The slope of the first portion was larger than the second portion, indicating that the intra-particle diffusion step was a gradual process (Fu et al. 2015). All the plots were nonlinear and did not pass through the origin, which implied that the adsorption process was complex and that intra-particle diffusion did not solely control the whole process (Qin et al. 2016). The related parameters of the intra-particle diffusion model are presented in Table 2, and the difference in the rate constants of Pb(II), Cd(II), and Mn(II) may be attributed to the nature and distribution of the active sites on the PVA-TA-βCD as well as the affinity between Pb(II), Cd(II), and Mn(II) and PVA-TA-βCD (Li et al. 2008).

The Boyd model is presented as follows:

$$\frac{q_t}{q_e} = G = 1 - \frac{6}{\pi^2}\exp(-B_t) \tag{8}$$

Equation (8) can be modified into the following form:

$$B_t = -0.4977\mathrm{In}(1-G) \tag{9}$$

where q_t (mg g^{-1}) and q_{te} (mg g^{-1}) are the adsorption amount at time t (min) and at equilibrium, respectively; G represents the fraction of Pb(II), Cd(II), and Mn(II) adsorbed at time t (min); and B_t is the mathematical function of G.

If the plots of the Boyd model are linear and pass through the origin, the rate-controlling step of the adsorption process is the intra-particle diffusion (Acharya et al. 2009). From Fig. 5b, it was observed that all the plots were linear but did not pass through the origin, which indicated that the adsorption of Pb(II), Cd(II), and Mn(II) onto the PVA-TA-βCD might be controlled by two or more steps (Senthil Kumar et al. 2014). The finding was consistent with the conclusion of the above model. Hence, film diffusion and intra-particle diffusion both played important roles in the adsorption process (Mohan et al. 2017).

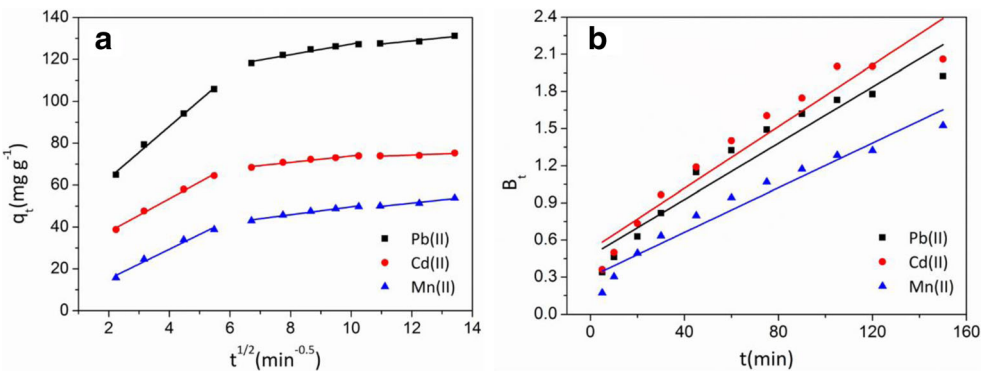

Fig. 5 **a** The intra-particle diffusion kinetic model and **b** Boyd model for Pb(II), Cd(II), and Mn(II) adsorption onto the PVA-TA-βCD (conditions: initial metal concentration, 100 mg L^{-1}; solution volume, 30 mL; adsorbent dosage, 0.02 g; solution pH, 5.5; contact time, 5–180 min; temperature, 298 K; and shaking speed, 120 rpm)

Table 2 Intra-particle diffusion kinetic model and Boyd model parameters for Pb(II), Cd(II), and Mn(II) on PVA-TA-βCD

Metals	Intra-particle diffusion kinetic model						Boyd model		
	Extragranular diffusion			Intergranular diffusion					
	R_1^2	$k_{i,1}$ (mg g^{-1} $min^{-0.5}$)	C_1	R_2^2	$k_{i,2}$ (mg g^{-1} $min^{-0.5}$)	C_2	k_{fd} (min^{-1})	Intercept	R^2
Pb(II)	0.992	12.426	38.386	0.948	2.540	101.898	0.011	0.473	0.921
Cd(II)	0.991	7.902	21.954	0.954	1.530	58.580	0.012	0.521	0.919
Mn(II)	0.976	7.092	1.059	0.970	1.895	30.750 k	0.009	0.302	0.946

Adsorption isotherms

In order to investigate the influence of different initial concentrations of the metal ions (25–300 mg L^{-1}) on the adsorption capacity, equilibrium measurements were performed. The Langmuir, Freundlich, and Sips models are the most prevalent models used to evaluate absorption characteristic.

The Langmuir isotherm is based on a monolayer and homogeneous adsorption (Vaghetti et al. 2009):

$$q_e = \frac{q_m K_L C_e}{1 + K_L C_e} \tag{10}$$

The Freundlich isotherm applies to multilayer sorption and a heterogeneous surface (Pang et al. 2011):

$$q_e = K_F C_e^{\frac{1}{n}} \tag{11}$$

The Sips model combines the characteristics of the Langmuir and Freundlich models and introduces a parameter (n_s) that is related to heterogeneity (Zhao et al. 2015a):

$$q_e = q_m \frac{(K_S C_e)^{\frac{1}{n_s}}}{1 + (K_S C_e)^{\frac{1}{n_s}}} \tag{12}$$

where C_e (mg L^{-1}) is the equilibrium concentration of the heavy metal ion, q_e (mg g^{-1}) is the amount of heavy metal ions absorbed at equilibrium, K_L (L mg^{-1}) is the Langmuir constant related to the adsorption energy, and q_m (mg g^{-1}) is the maximum adsorption capacity. K_F and n are the Freundlich constants related to the adsorption capacity and adsorption intensity, respectively. K_s is the Sips constant, and n_s represents the heterogeneity of the adsorbent; the closer the $1/n_s$ value to 1, the more uniform the adsorbent's surface is (Carvajal-Bernal et al. 2017).

The results assessing the adsorption of Pb(II), Cd(II), and Mn(II) onto the PVA-TA-βCD are shown in Table 3 and Fig. 6. Considering the values of the regression coefficient (R^2), the Langmuir and Sips models were found to fit the data for the three metal ions well. Comparing the values of RMSE and χ^2, the three models all displayed low errors, but the curve fitting via the Sips model was markedly better than the others. The sequence of the goodness of fit for the models was Sips > Langmuir > Freundlich. The maximum uptake capacities (q_m) calculated by the Langmuir and Sips models for Pb(II), Cd(II), and Mn(II) were 204.01, 127.87, and 105.52 mg g^{-1} and 199.11, 116.52, and 90.28 mg g^{-1}, respectively. The maximum adsorption capacities obtained in the experiment (191.02, 109.85, and 81.61 mg g^{-1}, respectively) were closer to the data calculated by the Sips model. These results indicated that the PVA-TA-βCD surface was heterogeneous (Zhao et al. 2015a; Oladipo et al. 2015). Additionally, in the Sips equation, when the n_s is close to unity, it can be reduced to the Langmuir equation. The values of n_s for the three metal ions were 0.903, 0.789, and 0.739, respectively, and these values are close to 1, indicating that one kind of group (might be –SH) was dominant and the others played a minor role in the adsorption.

The parameters of the Langmuir and Freundlich models also provide information regarding the PVA-TA-βCD. The K_L of the Langmuir model reflects the affinity of the

Table 3 Adsorption isotherm parameters for Pb(II), Cd(II), and Mn(II) on PVA-TA-βCD

Isotherms	Parameters	Pb(II)	Cd(II)	Mn(II)
Langmuir	Q_m (mg g^{-1})	204.01	127.87	105.52
	K_L (L mg^{-1})	0.137	0.028	0.016
	R^2	0.997	0.996	0.991
	RMSE	4.037	2.847	3.012
	χ^2	0.667	1.127	1.176
Freundlich	K_F (L mg^{-1})	59.698	17.252	8.320
	n	4.021	2.855	2.332
	R^2	0.896	0.944	0.943
	RMSE	25.129	10.194	7.694
	χ^2	31.154	9.381	6.963
Sips	q_m (mg g^{-1})	199.11	116.52	90.28
	K_s (L mg^{-1})	0.144	0.034	0.022
	n_s	0.903	0.789	0.739
	R^2	0.998	0.999	0.998
	RMSE	3.017	0.895	1.294
	χ^2	0.684	0.092	0.216

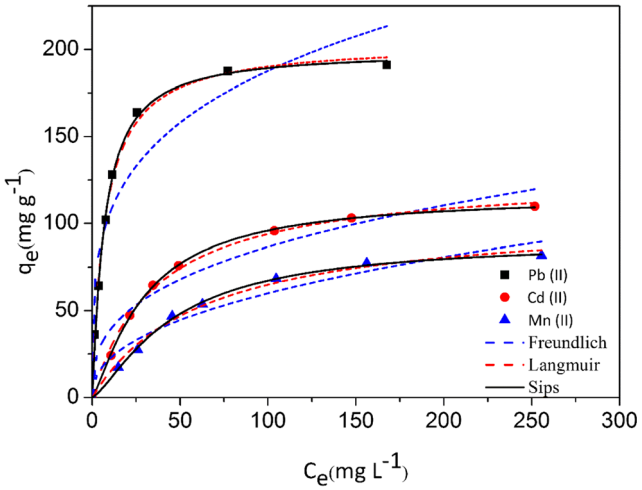

Fig. 6 Adsorption isotherms for Pb(II), Cd(II), and Mn(II) on the PVA-TA-βCD (conditions: initial metal concentration, 25–300 mg L^{-1}; solution volume, 30 mL; adsorbent dosage, 0.02 g; solution pH, 5.5; contact time, 180 min; temperature, 298 K; and shaking speed, 120 rpm)

adsorbent, and the order was Pb(II) (0.137) > Cd(II) (0.028) > Mn(II) (0.016), which was consistent with the sequence in which the adsorption amounts of the heavy metals had occurred (Qin et al. 2016). The values of the parameter n of the Freundlich model were greater than 1, which indicated that the adsorption of the three ions onto the PVA-TA-βCD was favorable and there was a high affinity between the metal ions and the PVA-TA-βCD. The comparison of the maximum adsorption capacities of the metals on the different adsorbents in a single metal system is shown in Table 4. Clearly, PVA-TA-βCD demonstrated a higher maximum adsorption capacity compared to the other presented sorbents. Additionally, for PVA-TA-βCD, the conditions for adsorption were easily meet and the contact time was limited, indicating PVA-TA-βCD had great potential for the removal of Pb(II), Cd(II), and Mn(II) from aqueous solutions.

Thermodynamic parameters

The Gibbs free energy change (ΔG^0), enthalpy change (ΔH^0), and entropy change (ΔS^0) are parameters that are commonly used to characterize the adsorption process. The parameters are expressed as follows:

$$\Delta G^0 = -RTInK_0 \tag{13}$$

$$InK_0 = \frac{\Delta S^0}{R} - \frac{\Delta H^0}{RT} \tag{14}$$

where R is the universal gas constant (8.314 J mol^{-1} K^{-1}), and T is the absolute temperature in Kelvin. K_0 $\left(K_0 = \frac{C_0 - C_e}{C_e} \times \frac{v}{m}\ mLg^{-1}\right)$ is the adsorption equilibrium constant. The calculated values of ΔG^0, ΔH^0, and ΔS^0 at 298, 308, 318, and 328 K with an initial concentration of 100 mg L^{-1} are shown in Fig. 7 and Table 5.

The free energy values (ΔG^0) for Pb(II), Cd(II), and Mn(II) were negative, indicating that the reactions promoting the absorption of the metal ions were spontaneous. We noted that the sequence of ΔG^0 of the metal ions was Pb(II) > Cd(II) > Mn(II), and these results are consistent with the arrangement of uptake capacities of the metal ions. Significantly, all the values of ΔG^0 increased slightly with increasing temperature, demonstrating that the reactions occurred more readily at higher temperatures. At the same time, the positive values of ΔH^0 also indicated that the reaction was endothermic. The positive values of ΔS^0 indicated that the randomness at the solid-liquid surface increased during the adsorption of Pb(II), Cd(II), and Mn(II) onto the PVA-TA-βCD (Zhao et al. 2015a).

Multi-component adsorption

At present, the composition of industrial wastewater is complex. In order to test the practicability of the PVA-TA-βCD for use in multi-metal solutions, the adsorption capacities of the PVA-TA-βCD in single, binary, and ternary solutions were investigated, and the results are depicted in Fig. 8. The uptake capacities of Pb(II), Cd(II), and Mn(II) in a single metal system were 129.45, 74.25, and 50.49 mg g^{-1}, respectively. In the binary metal solutions (Pb-Cd, Pb-Mn, and Cd-Mn), the metal ion adsorption capacities were different. In the Pb-Mn and Pb-Cd solutions, when the Cd(II) and Mn(II) were introduced, the adsorption capacities of Pb(II) exhibited no significant change (125.68 and 126.68 mg g^{-1}, respectively), whereas the adsorption capacities of Cd(II) and Mn(II) were obviously decreased (47.33 and 18.18 mg g^{-1}, respectively). In the Cd-Mn mixture, the uptake capacities of Cd(II) and Mn(II) both decreased markedly (58.20 and 27.06 mg g^{-1}, respectively) due to the competition between the two metal ions. In the ternary system, the uptake capacity of Pb(II) decreased slightly (122.76 mg g^{-1}), and the adsorption capacities of Cd(II) and Mn(II) decreased sharply and were lower than the adsorption capacities of the single or binary mixed solutions (41.4 and 15.42 mg g^{-1}, respectively)

The ratio of the adsorption capacities (R_q) was used to assess the adsorbent's behavior under competitive conditions in a multi-metallic aqueous solution:

$$R_q = \frac{q_{b,i}}{q_{m,i}} \tag{15}$$

where $q_{b,i}$ and $q_{m,i}$ are the uptakes of one metal ion in the multi-component system and mono-component system with the same initial concentration, respectively. As was previously reported (Chen et al. 2016a), (1) if $R_q > 1$, then the adsorption of the metal ion is promoted by the presence of other metal ions, which is called synergism; (2) if $R_q = 1$, then there is no effect on the adsorption capacity of the metal, which is called

Table 4 Comparison of the maximum adsorption capacities of Pb(II), Cd(II), and Mn(II) for various adsorbents

Sorbents	Maximum metal adsorption capacity (mg g^{-1})			Conditions	Ref.
	Pb(II)	Cd(II)	Mn(II)		
PVA/CNTs beads	196.3	–	–	pH = 6; 303 K Contact time: 540 min	Jing and Li 2016
CDpoly-MNPs	64.5	27.7	–	pH = 5.5; 298 K Contact time: 120 min	Badruddoza et al. 2013
Si-DTC	70.448	40.467	–	pH = 5 (Pb), 7 (Cd); 298 K Contact time: 60 min	Bai et al. 2011
β-CD polymer	196.42	136.43	–	pH = 5.0; 298 K Contact time: 5 min	He et al. 2017
EDTA-β-CD	–	124.325	–	Natural pH; r.t. Contact time: 600 min	Zhao et al. 2015a
ARM700	–	–	88.3	pH = 5; r.t. Contact time: 720 min	Chen et al. 2016b
PVA/CS	–	–	10.515	pH = 5; r.t. Contact time: 120 min	Abdeen et al. 2015
Synthesis of zeolite	–	–	66.93	pH = 6; 303 K Contact time: 180 min	Li et al. 2015
PVA-TA-βCD	199.110	116.522	90.275	pH = 5.5 (Pb, Cd, Mn); 298 K Contact time: 180 min	Present study

non-interaction; and (3) if $R_q < 1$, the presence of the other metal ions suppresses the adsorption of the metal ion, which is called antagonism.

The results are shown in Table 6. All values of R_q were less than 1, indicating that competition occurred between the ions, and this inhibited the adsorption of other ions by the PVA-TA-βCD. In addition, it was evident that the R_q value of Pb(II) in the multi-component system was close to 1, indicating that the presence of Cd(II) and Mn(II) suppressed the adsorption of Pb(II), although this influence was small. The adsorption capacity of the PVA-TA-βCD for most of the heavy metal ions decreased in the non-single systems, and this was attributed to the limited adsorption sites on the adsorbent and the competition of the ions for the adsorbent. Under these conditions, metals with a greater affinity were able to displace others with a weaker affinity to occupy the same adsorption sites.

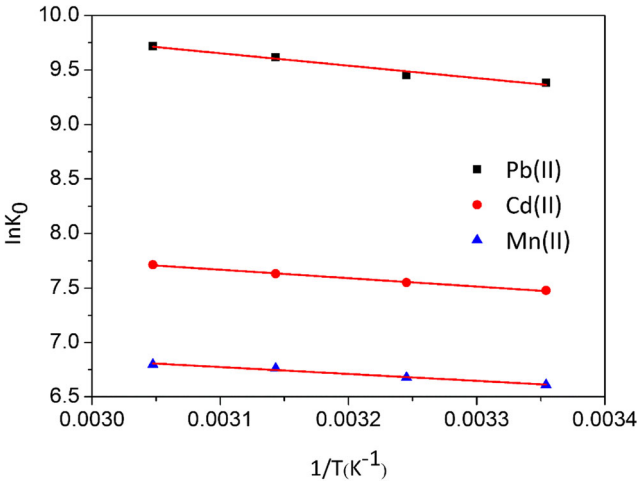

Fig. 7 Plots of In*K*c versus 1/*T* for the adsorption of Pb(II), Cd(II), and Mn(II) (conditions: initial metal concentration, 100 mg L^{-1}; solution volume, 30 mL; adsorbent dosage, 0.02 g; solution pH, 5.5; contact time, 180 min; temperature, 298–328 K; and shaking speed, 120 rpm)

Desorption and regeneration

From an economic and environmental viewpoint, a good adsorbent should possess excellent reproducibility when in actual operation. Desorption experiments were conducted to explore the regeneration of the PVA-TA-βCD using various different eluents (0.01 M HCl, 0.01 M HNO_3, and 0.1 M

Table 5 Thermodynamic parameters of Pb(II), Cd(II), and Mn(II) on PVA-TA-βCD at different temperatures

Metals	Temp. (K)	K_0 (mL g^{-1})	ΔG^0 (kJ mol^{-1})	ΔH^0 (kJ mol^{-1})	ΔS^0 (J mol^{-1} K^{-1})
Pb(II)	298	11880.91	− 23.246	9.486	109.661
	308	1231.5	− 24.203		
	318	14983.52	− 25.420		
	328	16615.94	− 26.501		
Cd(II)	298	1767.97	− 18.526	6.436	83.712
	308	1901.36	− 19.334		
	318	2062.95	− 20.178		
	328	2240.65	− 21.037		
Mn(II)	298	742.82	− 16.378	5.274	72.669
	308	794.982	− 17.101		
	318	864.439	− 17.878		
	328	896.166	− 18.538		

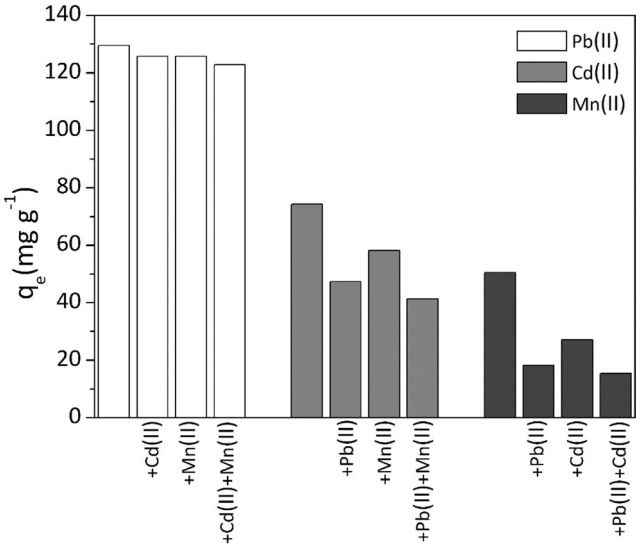

Fig. 8 Adsorption capacities of Pb(II), Cd(II), and Mn(II) from single, binary, and ternary mixtures (conditions: each metal concentration, 100 mg L^{-1}; solution volume, 30 mL; adsorbent dosage, 0.02 g; solution pH, 5.5; contact time, 180 min; temperature, 298 K; and shaking speed, 120 rpm)

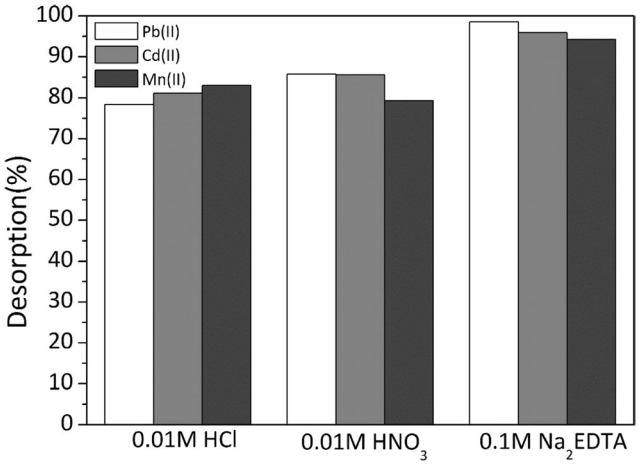

Fig. 9 Effects of the different eluents on the desorption efficiencies of Pb(II), Cd(II), and Mn(II) on PVA-TA-βCD

Na_2EDTA). For this process, 0.02 g of PVA-TA-βCD was immersed in 30 mL of 100 mg L^{-1} heavy metals for 180 min, and the heavy metal–loaded PVA-TA-βCD was then added to the abovementioned eluents for 480 min. The result of the desorption of the heavy metal ions using the three eluents is presented in Fig. 9. The desorption efficiency of EDTA was higher than the other buffers at Pb(II) (98.52%), Cd(II) (95.86%), and Mn(II) (94.28%). As EDTA can easily form stable metal-EDTA complexes with metals, the desorption kinetics and regeneration experiments for the adsorption of Pb(II), Cd(II), and Mn(II) were confirmed using a 0.1 M Na_2EDTA solution.

The tendencies for the desorption of Pb(II), Cd(II), and Mn(II), as shown in Fig. 10a, were the same as those for adsorption, and the desorption efficiencies were increased with contact time until reaching a desorption equilibrium at 480 min. It can be clearly seen that the Mn(II) ion reaches the desorption equilibrium prior to the Cd(II) and Pb(II) ions. Figure 10b and c shows the results of Pb(II), Cd(II), and Mn(II) over four adsorption-desorption cycles. The adsorption capacity was slightly decreased with the increasing number of cycle, from 131.25 to 122.08 mg g^{-1} for Pb(II), from 75.3 to 70.8 mg g^{-1} for Cd(II), and from 53.88 to 45.78 mg g^{-1} for Mn(II). These results clearly indicated PVA-TA-βCD had a good regeneration ability, supporting its potential for use in practical applications.

Adsorption mechanisms of Pb(II), Cd(II), and Mn(II) onto PVA-TA-βCD

FTIR

The FTIR results of the PVA-TA-βCD are shown in Fig. 11. The obvious peak at 3443.6 cm^{-1} belonged to –OH (Hallaji et al. 2015). A weak peak observed at 2563.78 cm^{-1} was attributed to the –SH stretching vibration and demonstrated that the –SH in the TA was successfully introduced onto the surface of the β-CD (Liang et al. 2009). The intensive absorption band occurring at 1726.47 cm^{-1} was attributed to the C=O stretching vibration of the carboxyl groups and ester groups (Hu et al. 2014). The absorbance spectra at 1402.78 cm^{-1} and 756.64 cm^{-1} corresponded to the symmetrical stretching vibration and formation vibration of $–COO^-$, respectively (Borsagli et al. 2015). These three peaks showed that the –COOH occurred on the adsorbent because the carboxyl group in the TA failed to completely react with the

Table 6 The ratio of adsorption capacities for Pb(II), Cd(II), and Mn(II) on PVA-TA-βCD in the multi-component system binary metal solutions

Metals	Single metal solution (mg g^{-1})	Binary metal solutions (mg g^{-1})						Ternary metal solutions (mg g^{-1})	
		Pb-Cd	R_q	Pb-Mn	R_q	Cd-Mn	R_q	Pb-Cd-Mn	R_q
Pb(II)	129.45	125.68	0.971	126.68	0.979	–	–	122.76	0.948
Cd(II)	74.25	47.33	0.637	–	–	58.20	0.784	41.4	0.558
Mn(II)	50.49	–	–	18.18	0.360	27.06	0.536	15.42	0.305

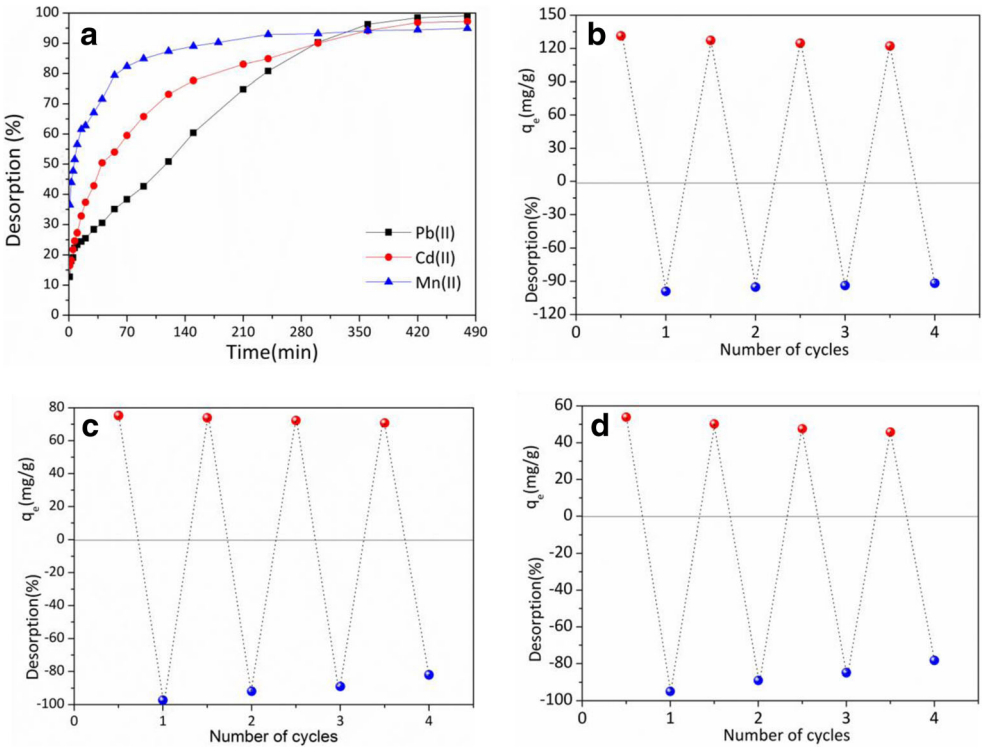

Fig. 10 **a** Effect of time on the desorption efficiency of Pb(II), Cd(II), and Mn(II) on PVA-TA-βCD. Regeneration studies **b** Pb(II), **c** Cd(II), and **d** Mn(II) (conditions: initial metal concentration, 100 mg L^{-1}; desorption agent, 0.1 M Na_2EDTA; pH, 5.5; and shaking speed, 120 rpm)

hydroxyl groups of the β-CD and PVA. The absorption bands at 1026.96 cm^{-1} and 1156.31 cm^{-1} were ascribed to the symmetrical stretching vibration of C–O–C (Badruddoza et al. 2013; Qin et al. 2016), and this group was generated by the reaction of the carboxyl groups of the TA with the hydroxyl groups of the β-CD and PVA during the thermal cross-linking.

After the Pb(II), Cd(II), and Mn(II) were loaded onto the PVA-TA-βCD (Figs. 12, 13, and 14), all the peaks differed from those prior to the adsorption. The –OH at 3443.6 cm^{-1} markedly shifted to 3427.46, 3422.16, and 3432.18 cm^{-1}, respectively. The –SH stretching vibration peak at 2563.78 cm^{-1} shifted to 2548.49 cm^{-1} for Pb(II), 2549.95 cm^{-1} for Cd(II), and 2550.14 cm^{-1} for Mn(II). The peak of C=O occurring at 1726.47 cm^{-1} shifted to 1722.21 cm^{-1} for Pb(II) and 1730.81 cm^{-1} for Cd(II). The two peaks of $–COO^-$ at 1402.78 cm^{-1} and 756.64 cm^{-1} shifted to 1399.88, 1403.04, and 1401.24 cm^{-1} and to 754.78, 755.57, and 755.48 cm^{-1}, respectively. The resulting peaks of –OH and –SH indicated

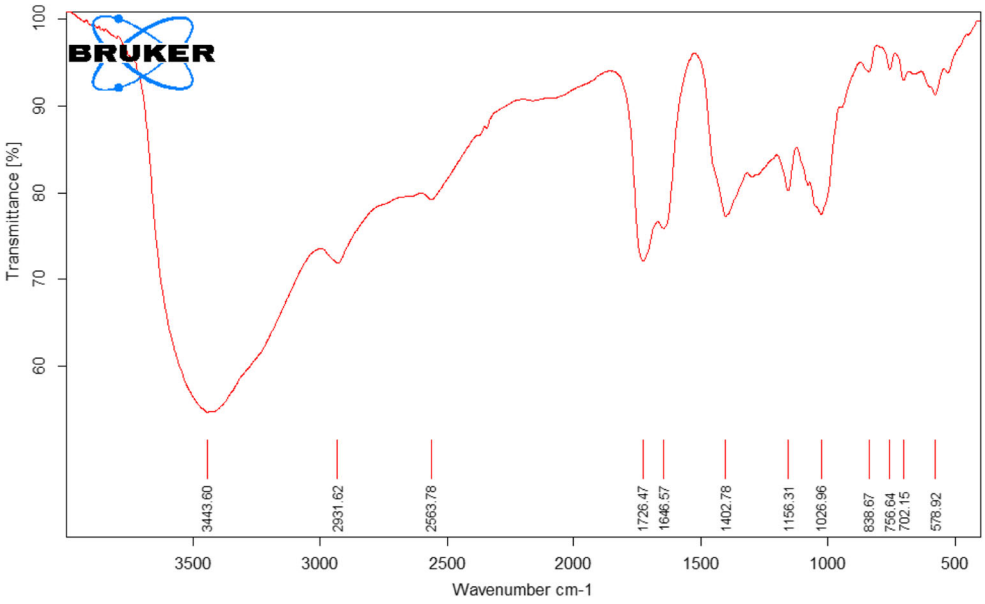

Fig. 11 FTIR spectra of PVA-TA-βCD

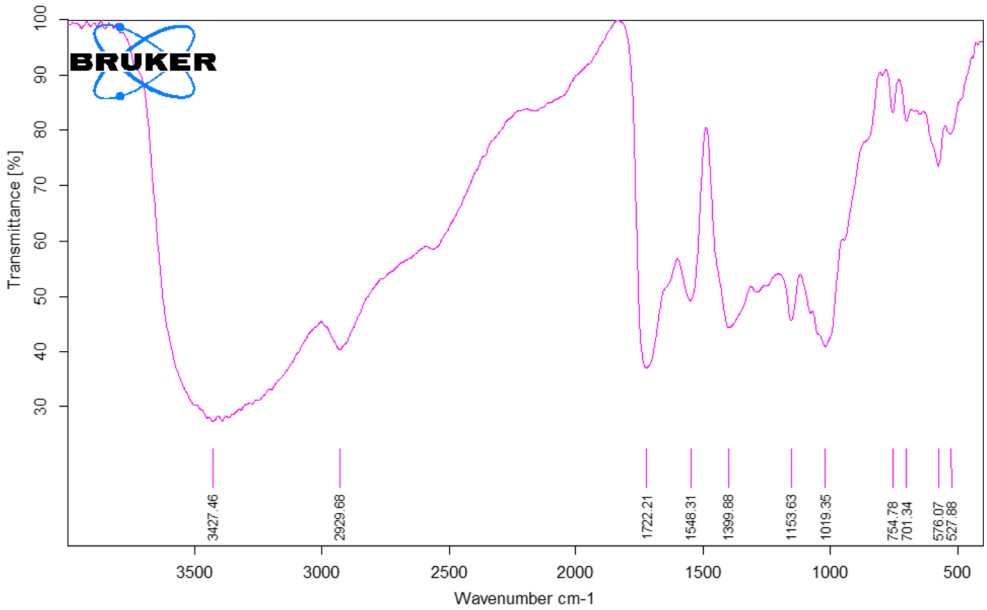

Fig. 12 FTIR spectra of PVA-TA-βCD after Pb(II) adsorption

they both reacted with the heavy metal ions. The peaks of C=O and $–COO^{-}$ changed little, demonstrating that the –COOH participates in the reaction, but it is not the main functional group that reacts with the heavy metals.

XPS

For further insight into the adsorption mechanism of Pb(II), Cd(II), and Mn(II) onto PVA-TA-βCD, the XPS spectra of the adsorbent before and after the metal ion adsorption were analyzed. The wide scan spectra of the pristine and heavy metal ions loaded onto the adsorbent are shown in Fig. 15a. It was evident that the main elements in the PVA-TA-βCD were O, C, and S. This also demonstrated that the functional group (–SH) was successfully introduced into the adsorbent, and these results were consistent with those obtained from the EDS and FTIR. The appearance of the new elements (Pb, Cd, and Mn) in the PVA-TA-βCD-M^{2+} (M: Pb, Cd, and Mn) indicated that the Pb(II), Cd(II), and Mn(II) were adsorbed onto the surface of the PVA-TA-βCD (Zhao et al. 2016).

The high-resolution scan of the O1s spectrum of the PVA-TA-βCD presented as four peaks at 532.01, 532.69, 533.02, and 533.83 eV, and these were assigned to –OH, O–C=O, C–O, and C–O–C, respectively (Wang et al. 2015; Ren et al. 2012; Li et al. 2016; Yu et al. 2007). After M^{2+}

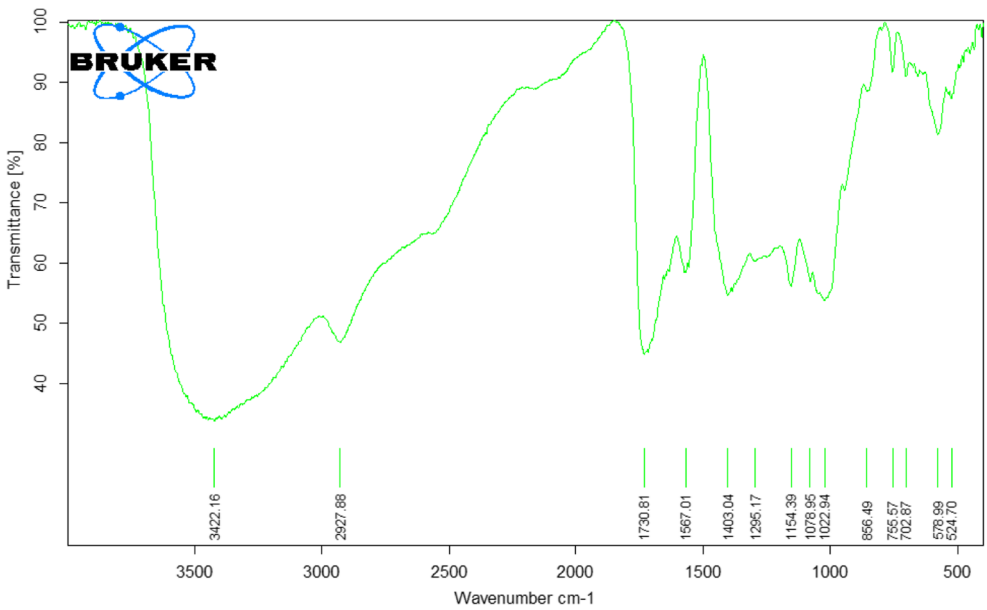

Fig. 13 FTIR spectra of PVA-TA-βCD after Cd(II) adsorption

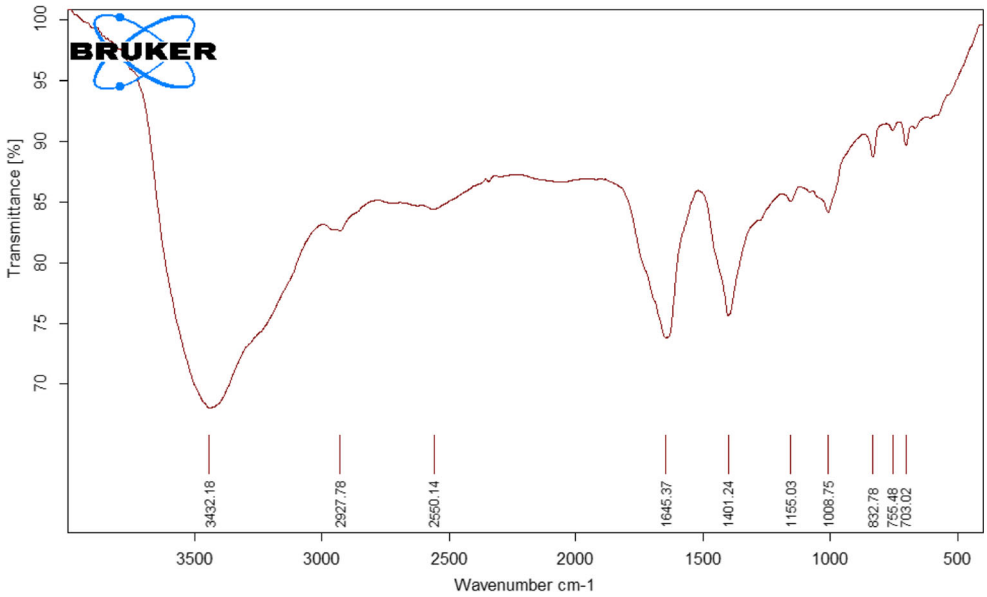

Fig. 14 FTIR spectra of PVA-TA-βCD after Mn(II) adsorption

adsorption onto the adsorbent, the binding energy of –OH, O–C=O, C–O, and C–O–C shifted to 532.25, 532.48, 532.76, and 533.68 eV (Fig. 15b). This indicated that both –OH and O–C=O of the PVA-TA-βCD were involved in the adsorption reaction with Pb(II), Cd(II), and Mn(II) to form the compound. The S2p spectra of the PVA-TA-βCD exhibited two peaks located at 164.25 and 165.38 eV. The mercapto group was readily oxidized, and its oxide form had the higher binding energy, so the peak at 164.25 eV was assigned to –SH (Zhu et al. 2012). After the adsorption of the three heavy metal ions, three new peaks appeared at 163.53, 163.68, and 164.37 eV (Liang et al. 2009; Ichimura and Sano 1991), indicating that the sulfhydryl groups in the TA were chelated with the metal ions (Fig. 15c). These results indicated that –OH, O–C=O, and –SH were involved in the reaction, and this was in agreement with the FTIR results. Additionally, from the results of XPS and FTIR, we can draw a conclusion that that the –SH group was dominant and the others played a minor role in the adsorption.

The species of the adsorbed heavy metal ions on the surface of the adsorbents are shown in Fig. 15d–f. The peaks at 138.95 eV and 143.80 eV were attributed to Pb 4f7/2 and Pb 4f5/2 (Wang et al. 2015; Ren et al. 2012), respectively, and the peaks at 405.80 eV and 412.55 eV were assigned to Cd 3d5/2 and Cd 3d3/2 (Chen et al. 2017; Liang et al. 2017), respectively. The peaks at 641.17 eV and 653.5 eV were ascribed to Mn2p 3/2 and Mn2p 1/2 (Chang et al. 2009; Ichimura and Sano 1991; Tan et al. 1991), respectively.

Selective adsorption

The different selective adsorption behaviors of Pb(II), Cd(II), and Mn(II) on PVA-TA-βCD could be explained by the characteristic properties of the metal ions. The electronegativity is higher for Pb(II) (2.33) than for Cd(II) (1.69) and Mn(II) (1.55), and the electronic attraction to counter-ions increases as the electronegativity increases. This property indicates that Pb(II) is more prone to be adsorbed by PVA-TA-βCD than Cd(II) or Mn(II) (Zhou et al. 2015). In the HSAB theory, Pb(II) is classified as a soft acid, whereas Cd(II) and Mn(II) are classified as intermediate acids (Wang and Chen 2009). Tsezos et al. (1996) found that a greater competition existed between ions of the same class and that the adsorption capacities of intermediate acids were affected by the presence of a soft acid, while intermediate acids cannot affect the adsorption process of a soft acid (Tsezos et al. 1996). The characteristics of metal ions affect their adsorption properties (e.g., atomic number, ionic potential, and ionic radius); however, since it is difficult to investigate the effect on a single factor, the concept of the covalent index ($X_m^2 r$) was proposed. $X_m^2 r$ reflects the importance of chelating interactions with ligands relative to ionic interactions (Jing et al. 2009). It was argued by Nieboer and Richardson (1980) that the value of $X_m^2 r$ is larger for a soft acid and that soft acids are more effective at binding to groups containing S (Nieboer and Richardson 1980). The PVA-TA-βCD was formed by cross-linking TA with β-CD and PVA; therefore, it contains a large amount of $–COO^-$ as well as $–S^-$ in the TA. The uptake capacity of Pb(II) was higher than the other metals because it easily combines with –SH to form a steady complex. The relationship between the uptake capacities and the $X_m^2 r$ for the three types of metal ions is shown in Fig. 16. A linear relationship exists between $X_m^2 r$ and q_e with a correlation coefficient (R^2) of 0.958.

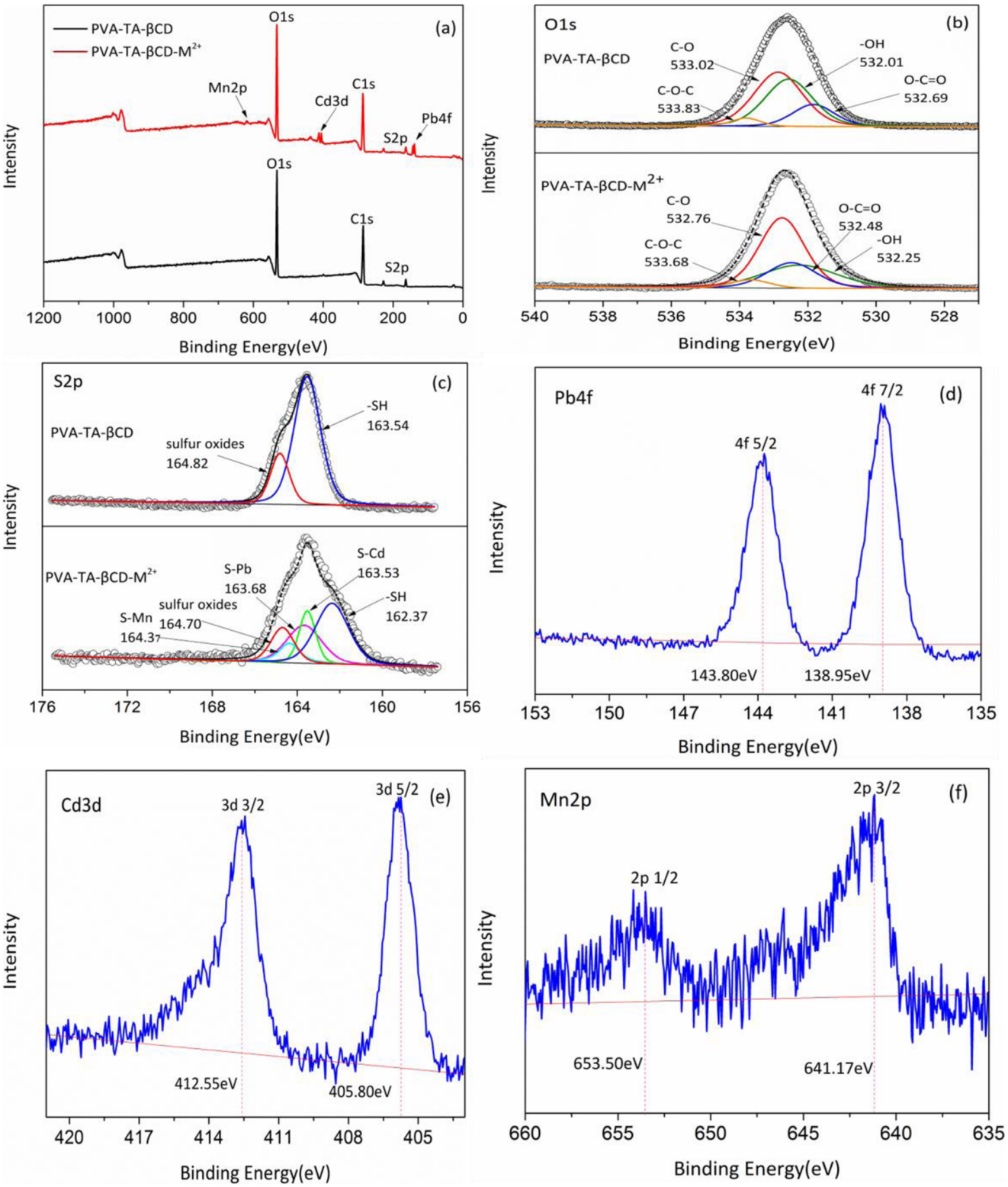

Fig. 15 XPS scan of PVA-TA-βCD before and after adsorption of Pb(II), Cd(II), and Mn(II). **a** Wide scan. **b** O1s for PVA-TA-βCD and PVA-TA-βCD-M^{2+} (M: Pb, Cd, Mn). **c** S2p for PVA-TA-βCD and PVA-TA-βCD-M^{2+} (M: Pb, Cd, Mn). **d** Pb 4f for PVA-TA-βCD-M^{2+}. **e** Cd 3d for PVA-TA-βCD-M^{2+}. **f** Mn2p for PVA-TA-βCD-M^{2+} (M: Pb, Cd, Mn)

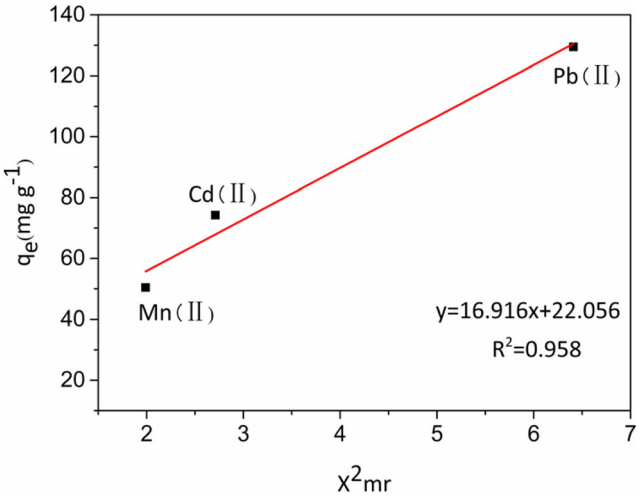

Fig. 16 Plots of the adsorption capacities versus the covalent indexes

Conclusion

The novel adsorbent PVA-TA-βCD was synthesized by combining β-CD, TA, and PVA for the purpose of removing heavy metal ions from liquid waste. The results of adsorption kinetics indicated that a chemical reaction occurred between the heavy metals and the adsorbents, and film diffusion and intra-particle diffusion both played important roles in the adsorption process. As for isotherm study, it showed a heterogeneous adsorption capacity of 199.11, 116.52, and 90.28 mg g^{-1} for the Pb(II), Cd(II), and Mn(II), respectively. There existed a competition between the ions in the multi-component system; however, owing to the stronger affinity of the PVA-TA-βCD for Pb(II) than Cd(II) and Mn(II), Pb(II) demonstrated a higher adsorption capacity, and its adsorption onto the PVA-TA-βCD was less affected by the addition of other metals. PVA-TA-βCD also demonstrated good reusability, as based on the regeneration experiments. The batch experiments and FTIR, XPS results indicated that the –SH group was dominant and the others played a minor role in the adsorption. Based on these observations, PVA-TA-βCD has demonstrated great potential in heavy metal ion adsorption from aqueous solutions.

Funding information This work was financially supported by the National Natural Science Foundation of China (Project No. 41562012).

References

Abdeen Z, Mohammad SG, Mahmoud MS (2015) Adsorption of Mn (II) ion on polyvinyl alcohol/chitosan dry blending from aqueous solution. Environmental Nanotechnology, Monitoring & Management 3:1–9. https://doi.org/10.1016/j.enmm.2014.10.001

Acharya J, Sahu JN, Sahoo BK, Mohanty CR, Meikap BC (2009) Removal of chromium(VI) from wastewater by activated carbon developed from Tamarind wood activated with zinc chloride. Chem Eng J 150:25–39. https://doi.org/10.1016/j.cej.2008.11.035

Ali RM, Hamad HA, Hussein MM, Malash GF (2016) Potential of using green adsorbent of heavy metal removal from aqueous solutions. Adsorption kinetics, isotherm, thermodynamic, mechanism and economic analysis. Ecol Eng 91:317–332. https://doi.org/10.1016/j.ecoleng.2016.03.015

Badruddoza AZM, Shawon ZBZ, Wei JDT, Hidajat K, Uddin MS (2013) Fe_3O_4/cyclodextrin polymer nanocomposites for selective heavy metals removal from industrial wastewater. Carbohydr Polym 91:322–332. https://doi.org/10.1016/j.carbpol.2012.08.030

Baghdadi M, Jafari A, Pardakhti A (2016) Removal of crystal violet from aqueous solutions using functionalized cellulose microfibers. A beneficial use of cellulosic healthcare waste. RSC Adv 6:61423–61433. https://doi.org/10.1039/c6ra08901a

Bai L, Hu H, Fu W, Wan J, Cheng X, Lei Z, Xiong L, Chen Q (2011) Synthesis of a novel silica-supported dithiocarbamate adsorbent and its properties for the removal of heavy metal ions. J Hazard Mater 195:261–275. https://doi.org/10.1016/j.jhazmat.2011.08.038

Borsagli FGLM, Mansur AAP, Chagas P, Oliveira LCA, Mansur HS (2015) O -carboxymethyl functionalization of chitosan: complexation and adsorption of Cd (II) and Cr (VI) as heavy metal pollutant ions. React Funct Polym 97:37–47. https://doi.org/10.1016/j.reactfunctpolym.2015.10.005

Carvajal-Bernal AM, Gomez-Granados F, Giraldo L, Moreno-Pirajan JC (2017) Application of the Sips model to the calculation of maximum adsorption capacity and immersion enthalpy of phenol aqueous solutions on activated carbons. Cent Eur J Chem 8:112–118. https://doi.org/10.5155/eurjchem.8.2.112-118.1556

Chang JK, Huang CH, Lee MT, Tsai WT, Deng MJ, Sun IW (2009) Physicochemical factors that affect the pseudocapacitance and cyclic stability of Mn oxide electrodes. Electrochim Acta 54:3278–3284. https://doi.org/10.1016/j.electacta.2008.12.042

Chen B, Liu Y, Chen S, Zhao X, Yue W, Pan X (2016a) Nitrogen-rich core/shell magnetic nanostructures for selective adsorption and separation of anionic dyes from aqueous solution. Environ Sci-Nano 3:670–681. https://doi.org/10.1039/c6en00022c

Chen H, Zheng J, Zhang Z, Long Q, Zhang Q (2016b) Application of annealed red mud to $Mn^{(2+)}$ ion adsorption from aqueous solution. Water Sci Technol 73(11):2761–2771. https://doi.org/10.2166/wst.2016.139

Chen G, Shah KJ, Shi L, Chiang PC (2017) Removal of Cd(II) and Pb(II) ions from aqueous solutions by synthetic mineral adsorbent. Performance and mechanisms. Appl Surf Sci 409:296–305. https://doi.org/10.1016/j.apsusc.2017.03.022

Crini G (2005) Recent developments in polysaccharide-based materials used as adsorbents in wastewater treatment. Prog Polym Sci 30:38–70. https://doi.org/10.1016/j.progpolymsci.2004.11.002

Feizi M, Jalali M (2015) Removal of heavy metals from aqueous solutions using sunflower, potato, canola and walnut shell residues. J Taiwan Inst Chem E 54:125–136. https://doi.org/10.1016/j.jtice.2015.03.027

Fu J, Chen Z, Wang M, Liu S, Zhang J, Zhang J, Han R, Xu Q (2015) Adsorption of methylene blue by a high-efficiency adsorbent (polydopamine microspheres). Kinetics, isotherm, thermodynamics and mechanism analysis. Chem Eng J 259:53–61. https://doi.org/10.1016/j.cej.2014.07.101

Girek T, Ciesielski W (2011) Polymerization of β-cyclodextrin with succinic anhydride and thermogravimetric study of the polymers. J

Incl Phenom Macro 69:439–444. https://doi.org/10.1007/s10847-010-9777-5

Grujić S, Vasić S, Čomić L, Ostojić A, Radojević I (2017) Heavy metal tolerance and removal potential in mixed-species biofilm. Water Sci Technol 76:806–812. https://doi.org/10.2166/wst.2017.248

Hallaji H, Keshtkar AR, Moosavian MA (2015) A novel electrospun PVA/ZnO nanofiber adsorbent for U(VI), Cu(II) and Ni(II) removal from aqueous solution. J Taiwan Inst Chem E 46:109–118. https://doi.org/10.1016/j.jtice.2014.09.007

He J, Li Y, Wang C, Zhang K, Lin D, Kong L, Liu J (2017) Rapid adsorption of Pb, Cu and Cd from aqueous solutions by β-cyclodextrin polymers. Appl Surf Sci 426:29–39. https://doi.org/10.1016/j.apsusc.2017.07.103

He C, Zhou Q, Duan Z, Xu X, Wang F, Li H (2018) One-step synthesis of a β-cyclodextrin derivative and its performance for the removal of Pb(II) from aqueous solutions. Res Chem Intermed 44:2983–2998. https://doi.org/10.1007/s11164-018-3289-0

Heidari A, Younesi H, Mehraban Z (2009) Removal of Ni(II), Cd(II), and Pb(II) from a ternary aqueous solution by amino functionalized mesoporous and nano mesoporous silica. Chem Eng J 153:70–79. https://doi.org/10.1016/j.cej.2009.06.016

Hu Q, Gao D, Pan H, Hao L, Wang P (2014) Equilibrium and kinetics of aniline adsorption onto crosslinked sawdust-cyclodextrin polymers. RSC Adv 4:857–860. https://doi.org/10.1039/c4ra05653a

Hu LQ, Dai L, Liu R, Si CL (2017) Lignin- graft -poly(acrylic acid) for enhancement of heavy metal ion biosorption. J Mater Sci 52:13689–13699. https://doi.org/10.1007/s10853-017-1463-1

Ichimura K, Sano M (1991) Electrical conductivity of layered transition-metal phosphorus trisulfide crystals. Synth Met 45:203–211

Jia Q, Zhang W, Li D, Liu Y, Che Y, Ma Q, Meng F (2016) Hydrazinolyzed cellulose-g-polymethyl acrylate as adsorbent for efficient removal of Cd(II) and Pb(II) ions from aqueous solution. Water Sci Technol 91:1378–1386. https://doi.org/10.2166/wst.2016.581

Jing L, Li X (2016) Facile synthesis of PVA/CNTs for enhanced adsorption of Pb^{2+} and Cu^{2+} in single and binary system. Desalin Water Treat 57:1–14. https://doi.org/10.1080/19443994.2015.1119739

Jing XS, Liu FQ, Yang X, Ling PP, Li LJ, Long C, Li AM (2009) Adsorption performances and mechanisms of the newly synthesized N,N′-di (carboxymethyl) dithiocarbamate chelating resin toward divalent heavy metal ions from aqueous media. J Hazard Mater 167:589–596. https://doi.org/10.1016/j.jhazmat.2009.01.020

Kyzas GZ, Siafaka PI, Pavlidou EG, Chrissafis KJ, Bikiaris DN (2015) Synthesis and adsorption application of succinyl-grafted chitosan for the simultaneous removal of zinc and cationic dye from binary hazardous mixtures. Chem Eng J 259:438–448. https://doi.org/10.1016/j.cej.2014.08.019

Li XM, Liao DX, Xu XQ, Yang Q, Zeng GM, Zheng W, Guo L (2008) Kinetic studies for the biosorption of lead and copper ions by *Penicillium simplicissimum* immobilized within loofa sponge. J Hazard Mater 159:610–615. https://doi.org/10.1016/j.jhazmat.2008.02.068

Li C, Zhong H, Wang S, Xue J, Zhang Z (2015) A novel conversion process for waste residue. Synthesis of zeolite from electrolytic manganese residue and its application to the removal of heavy metals. Colloid Surfaces A 470:258–267. https://doi.org/10.1016/j.colsurfa.2015.02.003

Li F, Li D, Li X, Liao J, Li S, Yang J, Yang Y, Tang J, Liu N (2016) Microorganism-derived carbon microspheres for uranium removal from aqueous solution. Chem Eng J 284:630–639. https://doi.org/10.1016/j.cej.2015.09.015

Liang X, Xu Y, Sun G, Wang L, Sun Y, Qin X (2009) Preparation, characterization of thiol-functionalized silica and application for sorption of Pb^{2+} and Cd^{2+}. Colloid Surface A 349:61–68. https://doi.org/10.1016/j.colsurfa.2009.07.052

Liang J, Li X, Yu Z, Zeng G, Luo Y, Jiang L, Yang Z, Qian Y, Wu H (2017) Amorphous MnO_2 modified biochar derived from aerobically composted swine manure for adsorption of Pb (II) and Cd (II). ACS Sustain Chem Eng 5:5049–5058. https://doi.org/10.1021/acssuschemeng.7b00434

Liu Y, Qian P, Yu Y, Yu B, Wang Y, Ye S, Chen Y (2018) Preparation and characterization of a novel hybrid chelating material for effective adsorption of Cu(II) and Pb(II). J Environ Sci-China 67:224–236. https://doi.org/10.1016/j.jes.2017.08.026

Luo S, Xu X, Zhou G, Liu C, Tang Y, Liu Y (2014) Amino siloxane oligomer-linked graphene oxide as an efficient adsorbent for removal of Pb(II) from wastewater. J Hazard Mater 274:145–155. https://doi.org/10.1016/j.jhazmat.2014.03.062

Mohan S, Kumar V, Singh DK, Hasan SH (2017) Effective removal of lead ions using graphene oxide-MgO nanohybrid from aqueous solution. Isotherm, kinetic and thermodynamic modeling of adsorption. J Environ Chem Eng 5:2259–2273. https://doi.org/10.1016/j.jece.2017.03.031

Moulahcene L, Skiba M, Senhadji O, Milon N, Benamor M, Lahiani-Skiba M (2015) Inclusion and removal of pharmaceutical residues from aqueous solution using water-insoluble cyclodextrin polymers. Chem Eng Res Des 97:145–158. https://doi.org/10.1016/j.cherd.2014.08.023

Nieboer E, Richardson DHS (1980) The replacement of the nondescript term 'heavy metals' by a biologically and chemically significant classification of metal ions. Environ Pollut 1:3–26

Oladipo AA, Gazi M, Yilmaz E (2015) Single and binary adsorption of azo and anthraquinone dyes by chitosan-based hydrogel. Selectivity factor and Box-Behnken process design. Chem Eng Res Des 104:264–279. https://doi.org/10.1016/j.cherd.2015.08.018

Ozdes D, Duran C, Senturk HB (2011) Adsorptive removal of Cd(II) and Pb(II) ions from aqueous solutions by using Turkish illitic clay. J Environ Manag 92:3082–3090. https://doi.org/10.1016/j.jenvman.2011.07.022

Pang Y, Zeng G, Tang L, Zhang Y, Liu Y, Lei X, Li Z, Zhang J, Xie G (2011) PEI-grafted magnetic porous powder for highly effective adsorption of heavy metal ions. Desalination 281:278–284. https://doi.org/10.1016/j.desal.2011.08.001

Qin X, Zhou J, Huang A, Guan J, Zhang Q, Huang Z, Hu H, Zhang Y, Yang M, Wu J (2016) A green technology for the synthesis of cellulose succinate for efficient adsorption of Cd(II) and Pb(II) ions. RSC Adv 6:26817–26825. https://doi.org/10.1039/c5ra27280g

Ren Y, Li N, Feng J, Luan T, Wen Q, Li Z, Zhang M (2012) Adsorption of Pb(II) and Cu(II) from aqueous solution on magnetic porous ferrospinel $MnFe_2O_4$. J Colloid Interface Sci 367:415–421. https://doi.org/10.1016/j.jcis.2011.10.022

Senthil Kumar P, Palaniyappan M, Priyadharshini M, Vignesh AM, Thanjiappan A, Sebastina AFP, Tanvir Ahmed R, Srinath R (2014) Adsorption of basic dye onto raw and surface-modified agricultural waste. Environ Prog Sustain 33:87–98. https://doi.org/10.1002/ep.11756

Tan BJ, Klabunde KJ, Sherwood PMA (1991) XPS studies of solvated metal atom dispersed (SMAD) catalysts. Evidence for layered cobalt-manganese particles on alumina and silica. JAMA 113:855–861

Tsezos M, Remoudaki E, Angelatou V (1996) A study of the effects of competing ions on the biosorption of metals. Int Biodeterior Biodegrad 38:19–29

Vaghetti JCP, Lima EC, Royer B, Cunha BMD, Cardoso NF, Brasil JL, Dias SLP (2009) Pecan nutshell as biosorbent to remove Cu(II), Mn(II) and Pb(II) from aqueous solutions. J Hazard Mater 162:270–280. https://doi.org/10.1016/j.jhazmat.2008.05.039

Wang J, Chen C (2009) Biosorbents for heavy metals removal and their future. Biotechnol Adv 27:195–226. https://doi.org/10.1016/j.biotechadv.2008.11.002

Wang P, Du M, Zhu H, Bao S, Yang T, Zou M (2015) Structure regulation of silica nanotubes and their adsorption behaviors for heavy metal ions. PH effect, kinetics, isotherms and mechanism. J Hazard Mater 286:533–544. https://doi.org/10.1016/j.jhazmat.2014.12.034

Wang N, Xu X, Li H, Wang Q, Yuan L, Yu H (2017) High performance and prospective application of xanthate-modified thiourea chitosan sponge-combined *Pseudomonas putida* and *Talaromyces amestolkiae* biomass for Pb(II) removal from wastewater. Bioresour Technol 233:58–66. https://doi.org/10.1016/j.biortech.2017.02.069

Xu M, Zhang Y, Zhang Z, Shen Y, Zhao M, Pan G (2011) Study on the adsorption of Ca^{2+}, Cd^{2+} and Pb^{2+} by magnetic Fe_3O_4 yeast treated with EDTA dianhydride. Chem Eng J 168:737–745. https://doi.org/10.1016/j.cej.2011.01.069

Xu R, Zhou G, Tang Y, Chu L, Liu C, Zeng Z, Luo S (2015) New double network hydrogel adsorbent. Highly efficient removal of Cd(II) and Mn(II) ions in aqueous solution. Chem Eng J 275:179–188. https://doi.org/10.1016/j.cej.2015.04.040

Yu J, Tong M, Sun X, Li B (2007) A simple method to prepare poly(amic acid)-modified biomass for enhancement of lead and cadmium adsorption. Biochem Eng J 33:126–133. https://doi.org/10.1016/j.bej.2006.10.012

Yu HZ, Yang YM, Zhang L, Dang ZM, Hu GH (2014) Quantum-chemical predictions of pKa's of thiols in DMSO. J Phys Chem A 118:606–622. https://doi.org/10.1021/jp410274n

Zhao F, Repo E, Yin D, Meng Y, Jafari S, Sillanpää M (2015a) EDTA-cross-linked β-cyclodextrin. An Environmentally friendly bifunctional adsorbent for simultaneous adsorption of metals and cationic dyes. Environ Sci Technol 49:10570–10580. https://doi.org/10.1021/acs.est.5b02227

Zhao R, Wang Y, Li X, Sun B, Jiang Z, Wang C (2015b) Water-insoluble sericin/β-cyclodextrin/PVA composite electrospun nanofibers as effective adsorbents towards methylene blue. Colloid Surface B 136:375–382. https://doi.org/10.1016/j.colsurfb.2015.09.038

Zhao D, Yu Y, Chen JP (2016) Treatment of lead contaminated water by a PVDF membrane that is modified by zirconium, phosphate and PVA. Water Res 101:564–573. https://doi.org/10.1016/j.watres.2016.04.078

Zhou D, Kim DG, Ko SO (2015) Heavy metal adsorption with biogenic manganese oxides generated by *Pseudomonas putida* strain MnB1. J Ind Eng Chem 24:132–139. https://doi.org/10.1016/j.jiec.2014.09.020

Zhu Y, Hu J, Wang J (2012) Competitive adsorption of Pb(II), Cu(II) and Zn(II) onto xanthate-modified magnetic chitosan. J Hazard Mater 221-222:155–161. https://doi.org/10.1016/j.jhazmat.2012.04.026